Journal of Geophysical Research - Space Physics

Supporting Information for

Cluster Curlometry Limitations in the Ring Current Region

T. B. Keebler[1], M. W. Liemohn[1], N. Y. Ganushkina[1,2]

[1] Department of Climate and Space Sciences and Engineering, University of Michigan, Ann Arbor, MI.

[2] Space Research and Observation Technologies, Space and Earth Observation Centre, Finnish Meteorological Institute, Helsinki, Finland

Contents of this file

Figures S1 to S20

Additional Supporting Information (Files uploaded separately)

Captions for Movies S1 to S2

Introduction

The plots and animations herein supplement the material in the article by providing enhanced visualization and additional method verification. The first set of figures verify the correct operation of the curlometer script used for this study. Be careful to note that both vertical and horizontal axes are scaled to show detail and are not necessarily the same for comparable plots. These are followed by plots to be compared directly with selected figures from previous studies, with detailed descriptions of the differences in computation and generation. Finally, two animations are provided for cases involving the tetrahedron rotation and the generation of false currents. These animations add clarity to a complex process that is difficult to represent in stationary plots. The animation files are in the GIF format.

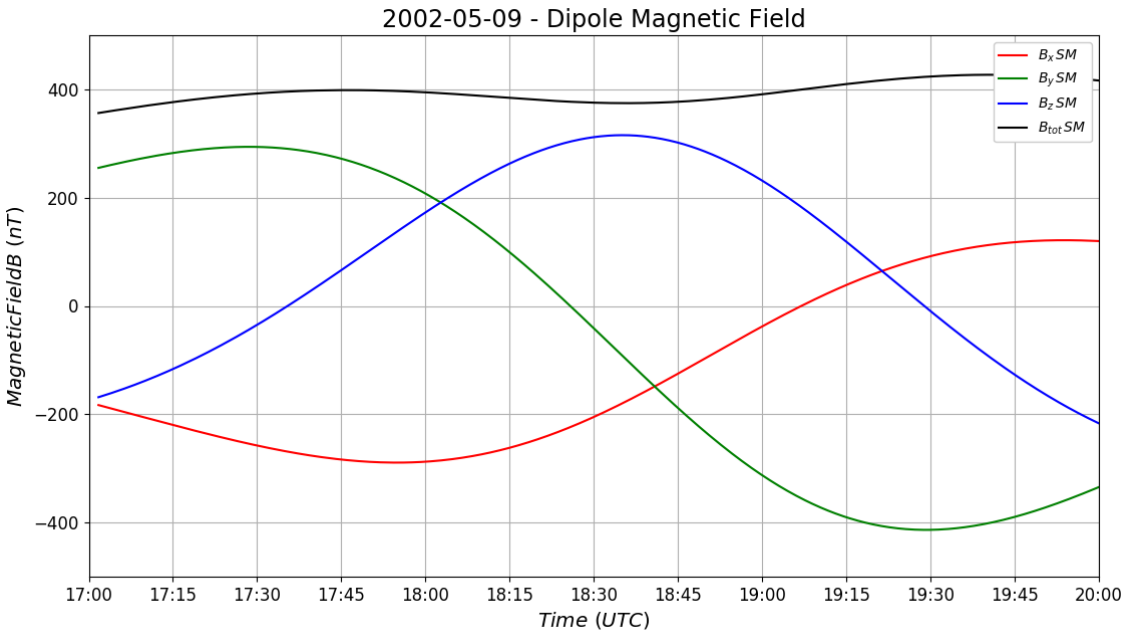

Figure S1. 9 May 2002 perigee pass with magnetometer data replaced by a simple approximation of Earth's dipole field.

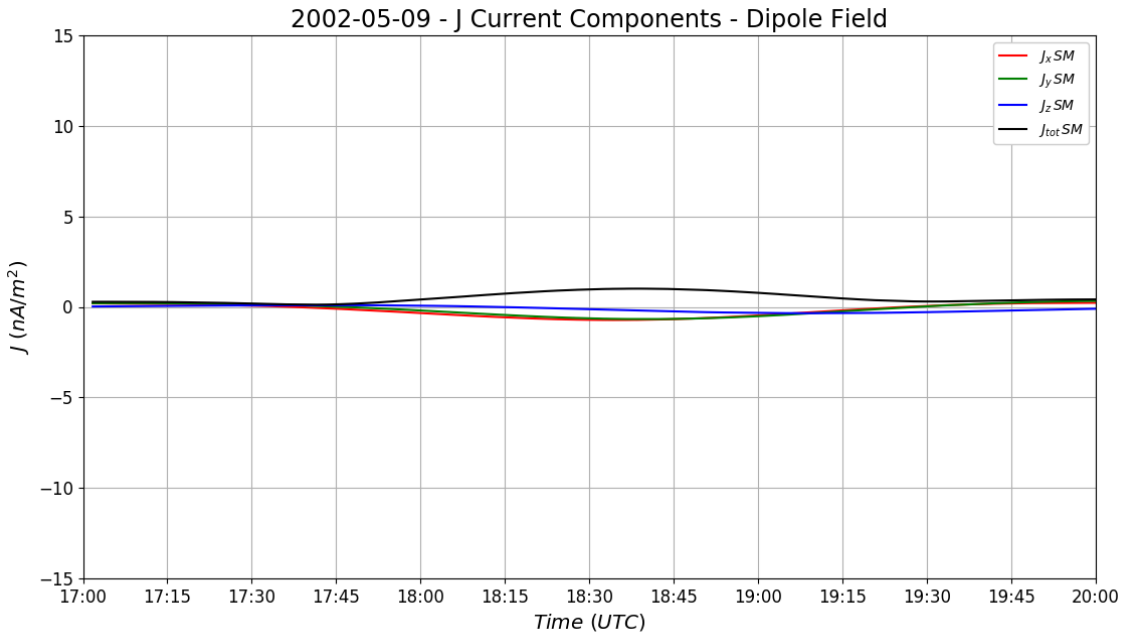

Figure S2. Curlometer currents output from the 9 May 2002 perigee pass with magnetometer data replaced by a simple approximation of Earth's dipole field.

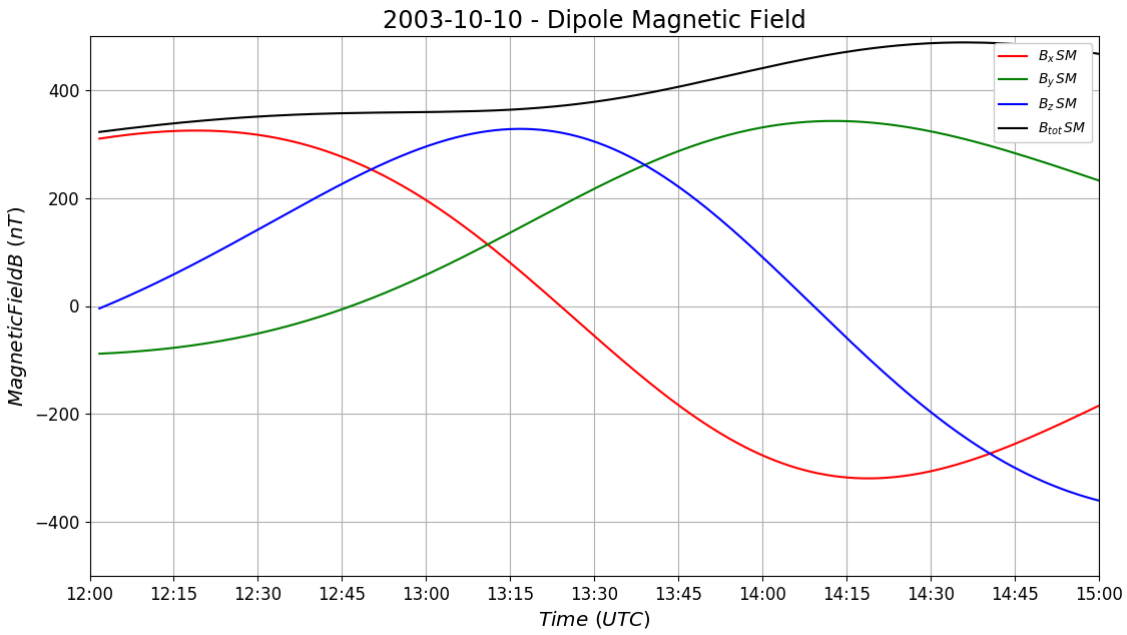

Figure S3. 10 October 2003 perigee pass with magnetometer data replaced by a simple approximation of Earth's dipole field.

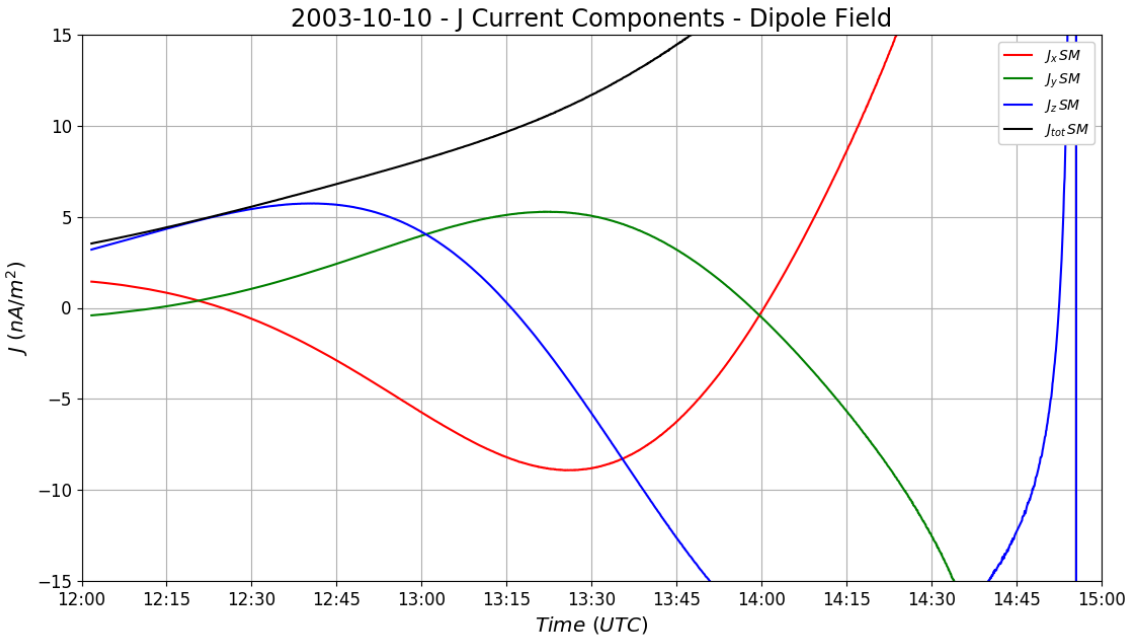

Figure S4. Curlometer currents output from the 10 October 2003 perigee pass with magnetometer data replaced by a simple approximation of Earth's dipole field.

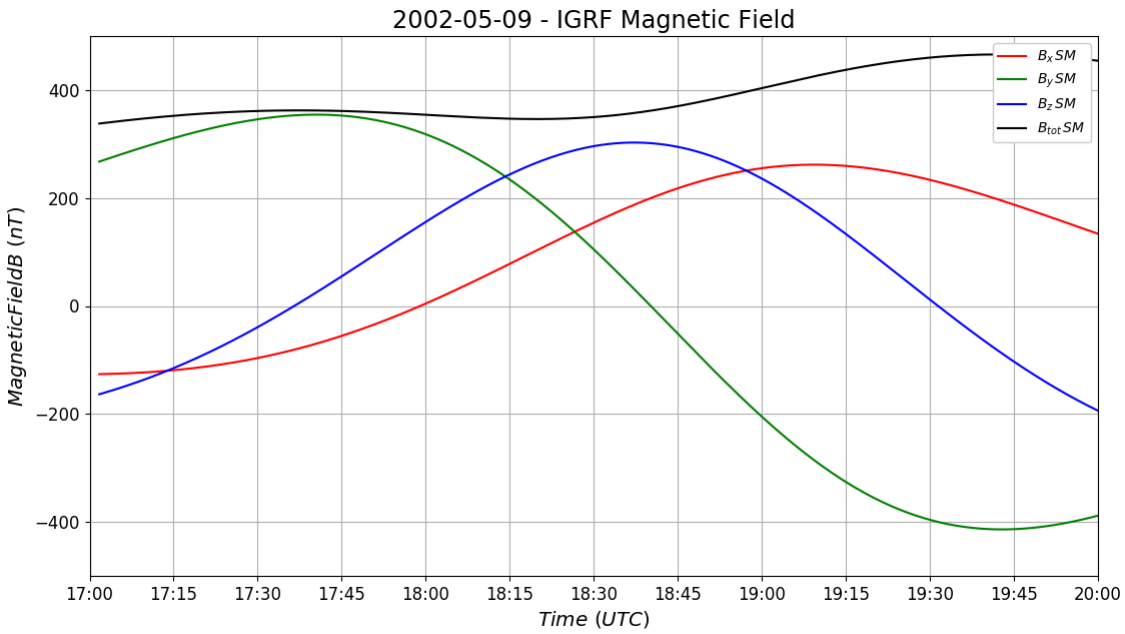

Figure S5. 9 May 2002 perigee pass with magnetometer data replaced by the International Geomagnetic Reference Field (IGRF) magnetic environment.

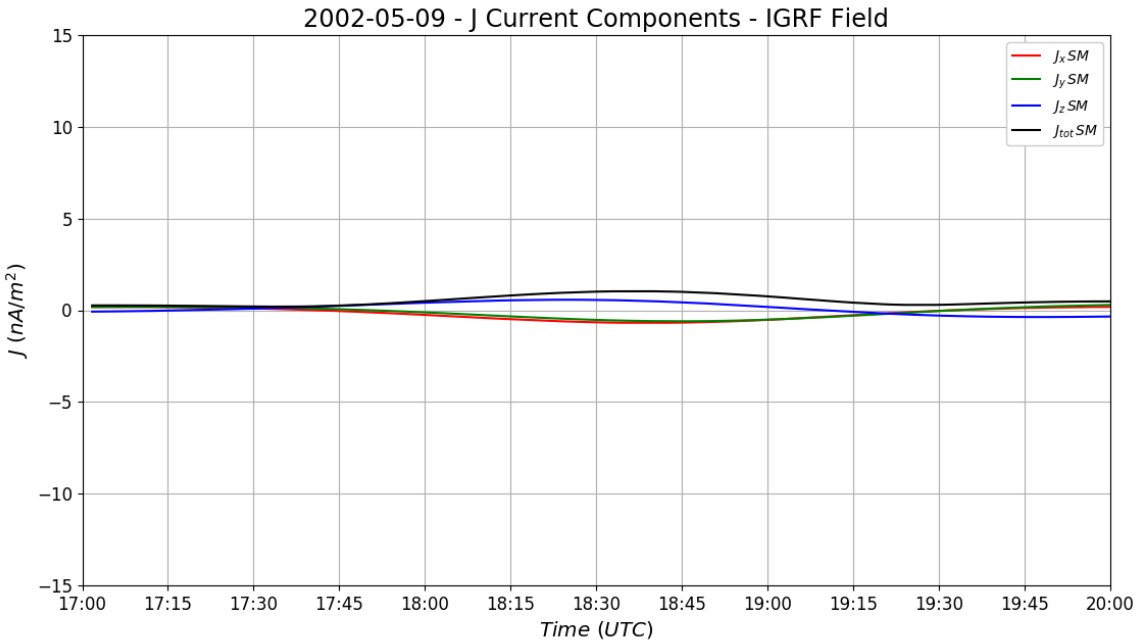

Figure S6. Curlometer currents output from the 9 May 2002 perigee pass with magnetometer data replaced by the IGRF magnetic environment.

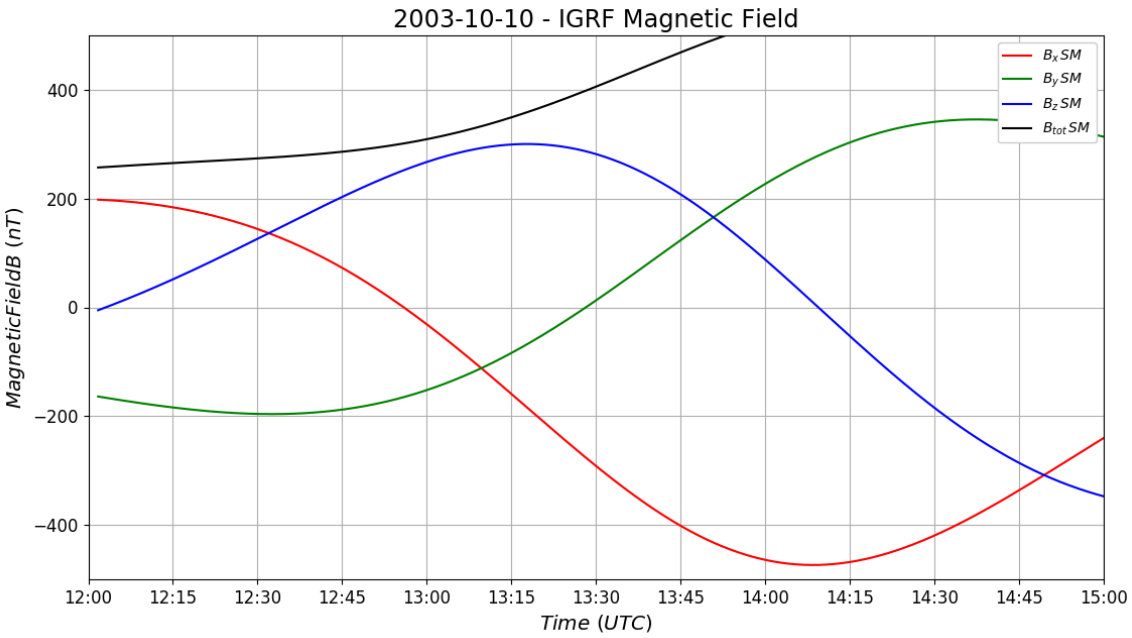

Figure S7. 10 October 2003 perigee pass with magnetometer data replaced by the IGRF magnetic environment.

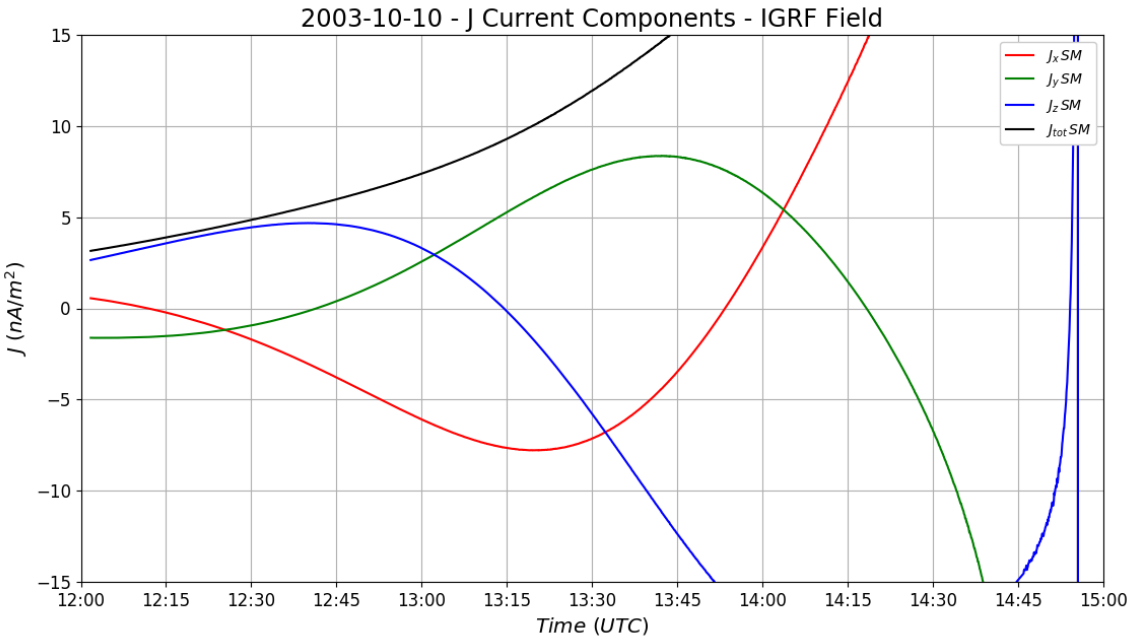

Figure S8. Curlometer currents output from the 10 October 2003 perigee pass with magnetometer data replaced by the IGRF magnetic environment.

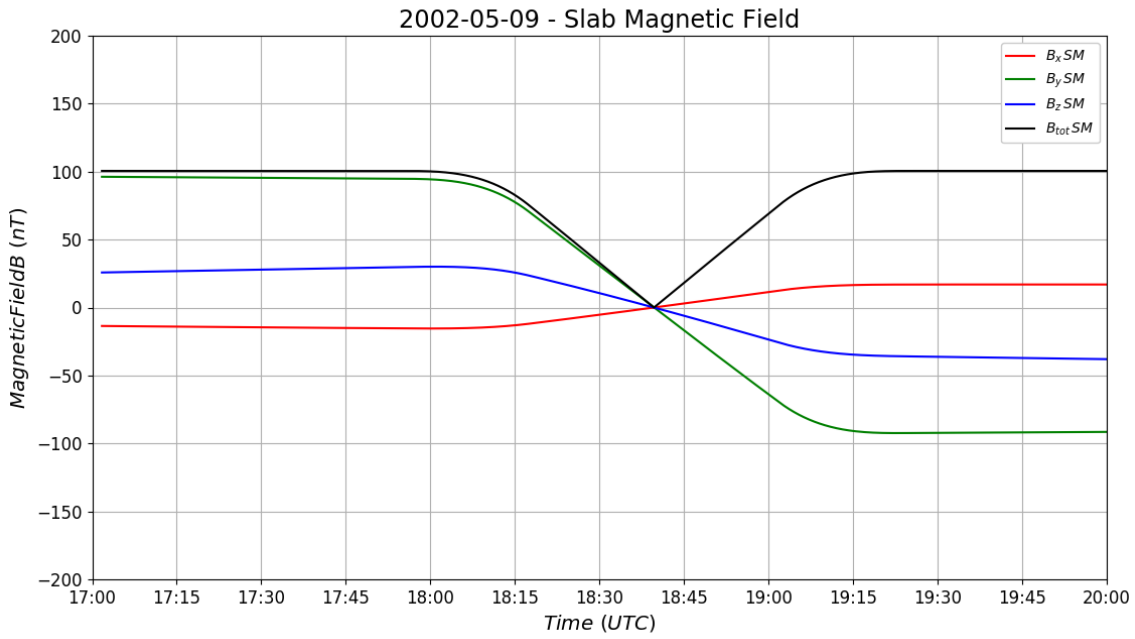

Figure S9. 9 May 2002 perigee pass with magnetometer data replaced by a simulated infinite current sheet (slab) in the z = 0 plane. The simulated slab current is constant over a finite thickness larger than the tetrahedron size, and tapers quadratically to either side.

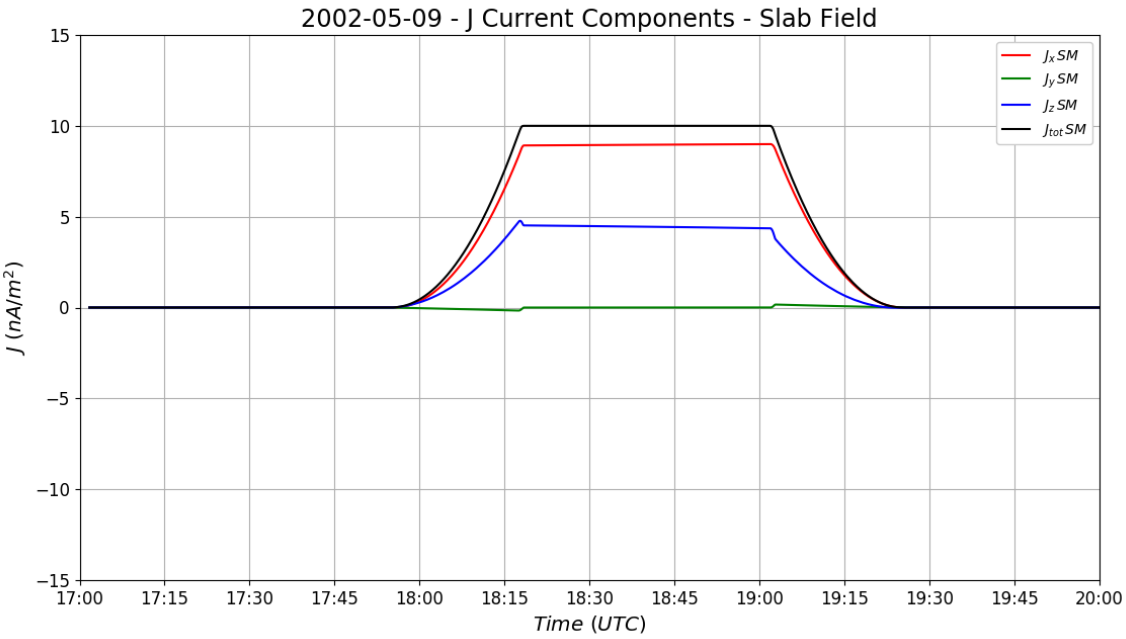

Figure S10. Curlometer currents output from the 9 May 2002 perigee pass with magnetometer data replaced by a simulated infinite current sheet in the z = 0 plane. The simulated slab current is constant over a finite thickness larger than the tetrahedron size, and tapers quadratically to either side. Note that the black current captures the imposed simulation current almost perfectly at 10 nA/m^2.

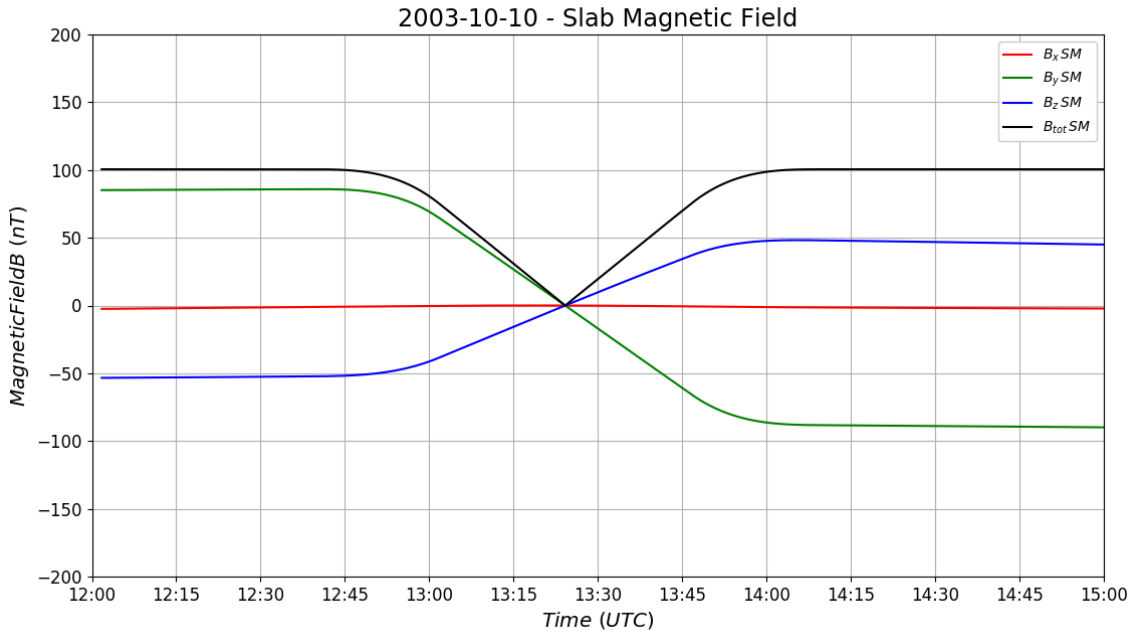

Figure S11. 10 October 2003 perigee pass with magnetometer data replaced by a simulated infinite current sheet (slab) in the z = 0 plane. The simulated slab current is constant over a finite thickness larger than the tetrahedron size, and tapers quadratically to either side.

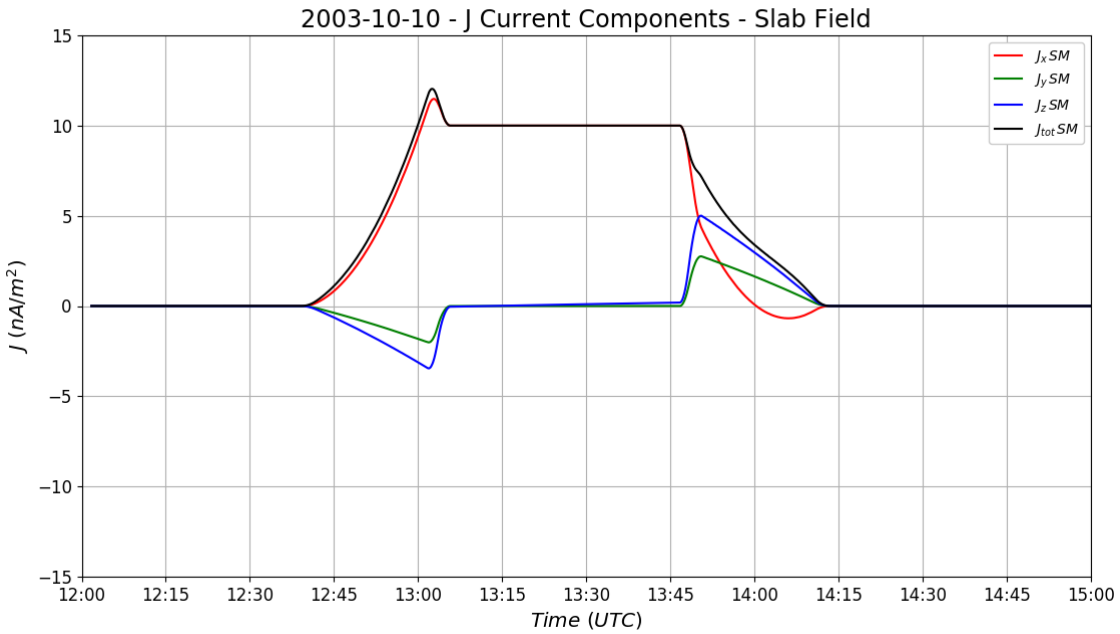

Figure S12. Curlometer currents output from the 10 October 2003 perigee pass with magnetometer data replaced by a simulated infinite current sheet in the z = 0 plane. The simulated slab current is constant over a finite thickness larger than the tetrahedron size, and tapers quadratically to either side. Note that the black current captures the imposed simulation current almost perfectly at 10 nA/m^2. Also note that, while in the sharp gradients to either side, the curlometer technique becomes inaccurate in all components.

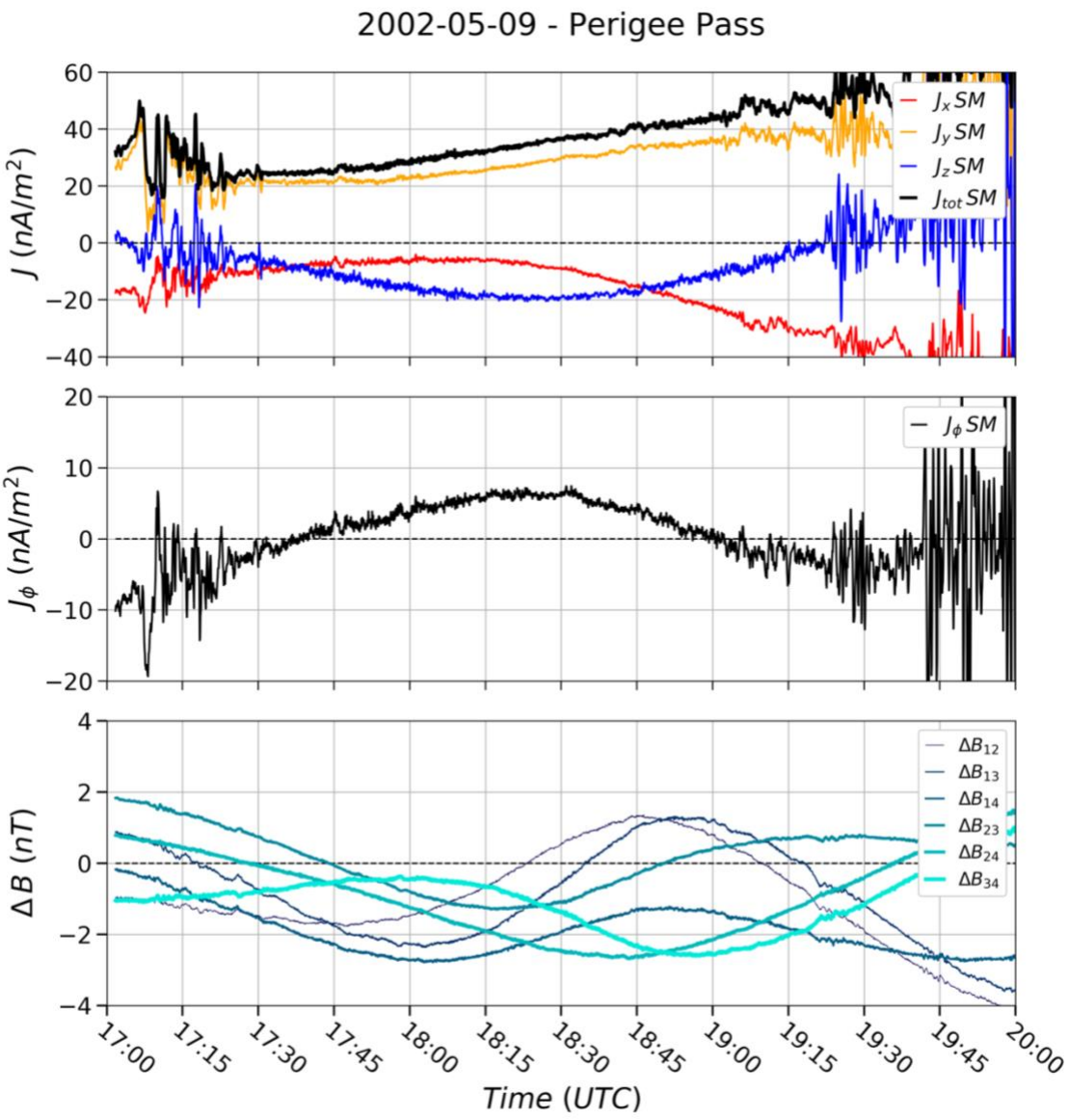

Figure S13. Investigation of instrument sensitivity for Cluster tetrahedron. Using the 9 May 2002 perigee pass, the magnetometer resolution of 0.125 nT was subtracted uniformly in time from the Cluster 1 spacecraft, chosen as the most irregular in the direction of the gradient for largest effect. The curlometer output of the modified magnetic data showed a decrease of about 2 nT in the azimuthal current. Compare Figure S13 to Figure S14, Figure S15, and Figure 1 in the paper.

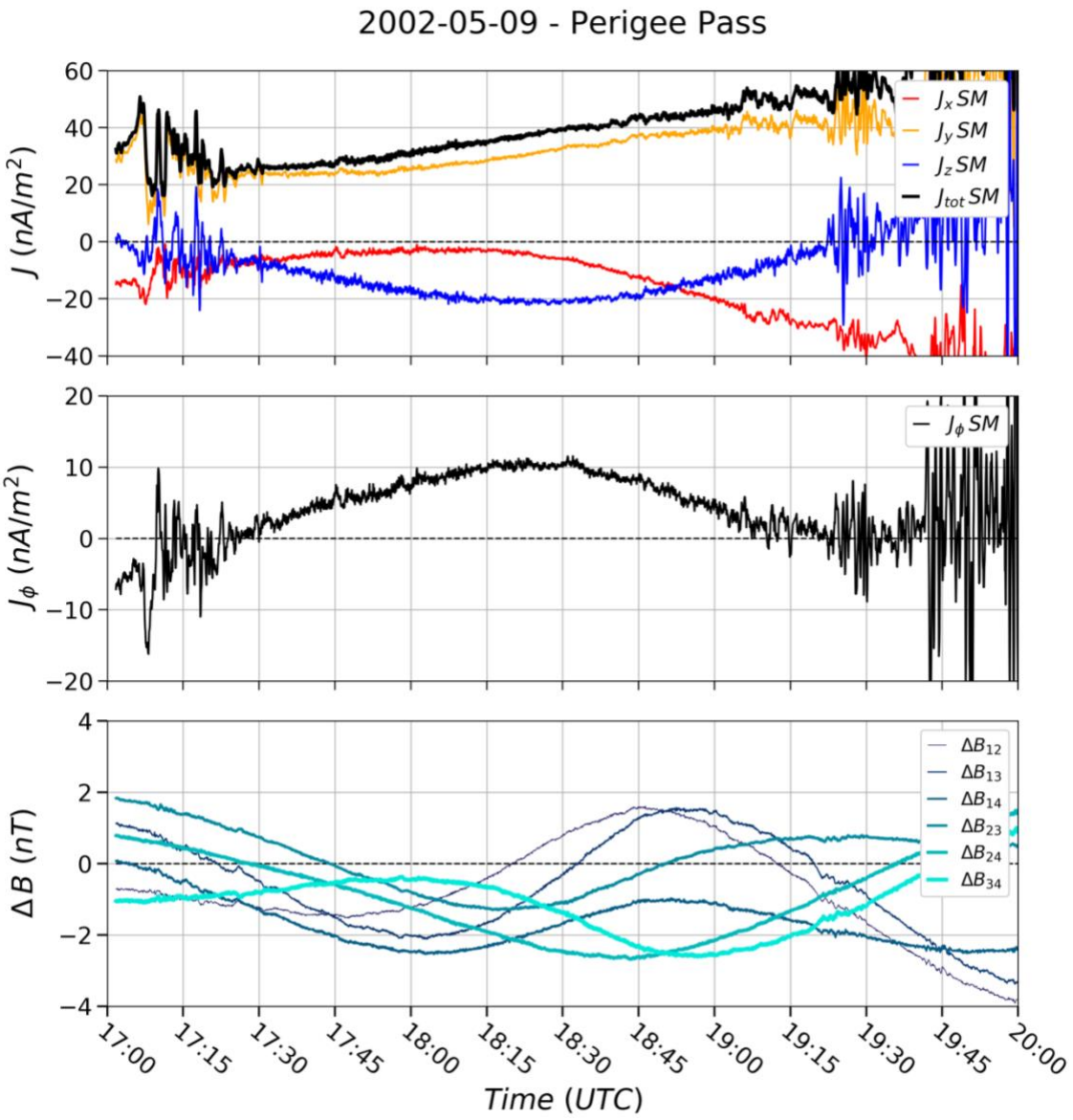

Figure S14. Investigation of instrument sensitivity for Cluster tetrahedron. Using the 9 May 2002 perigee pass, the magnetometer resolution of 0.125 nT was added uniformly in time from the Cluster 1 spacecraft, chosen as the most irregular in the direction of the gradient for largest effect. The curlometer output of the modified magnetic data showed an increase of about 1 nT in the azimuthal current. Compare Figure S14 to Figure S13, Figure S15, and Figure 1 in the paper.

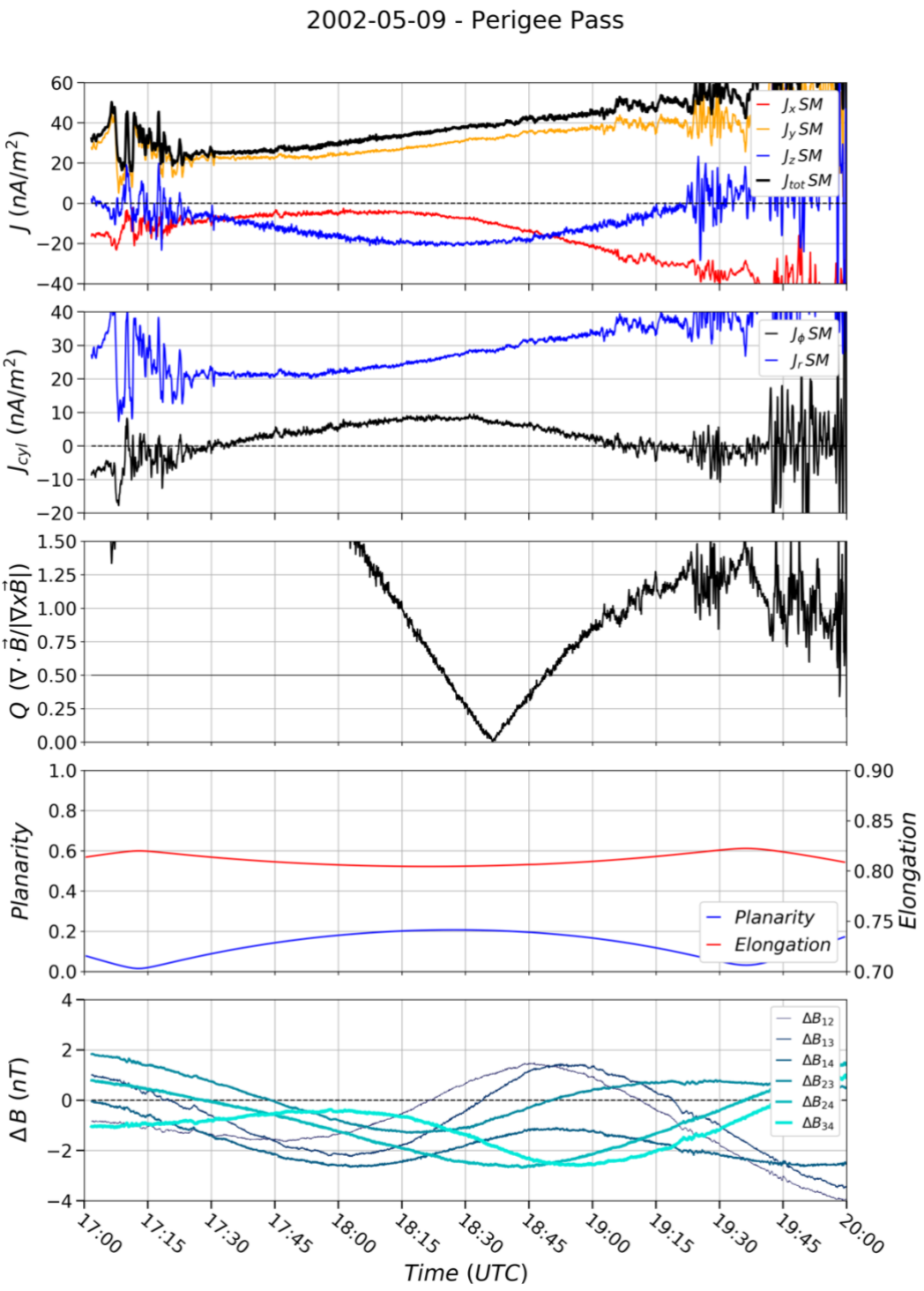

Figure S15. Full parameter consideration for the 9 May 2002 perigee pass. The panels from top to bottom depict:

- Cartesian and total currents in SM coordinates
- Azimuthal and radial current components in SM/local cylindrical coordinates
- Tetrahedron quality parameter Q

- Tetrahedron geometry factors elongation (E) and planarity (P)
- Magnetic field differences between spacecraft pairs

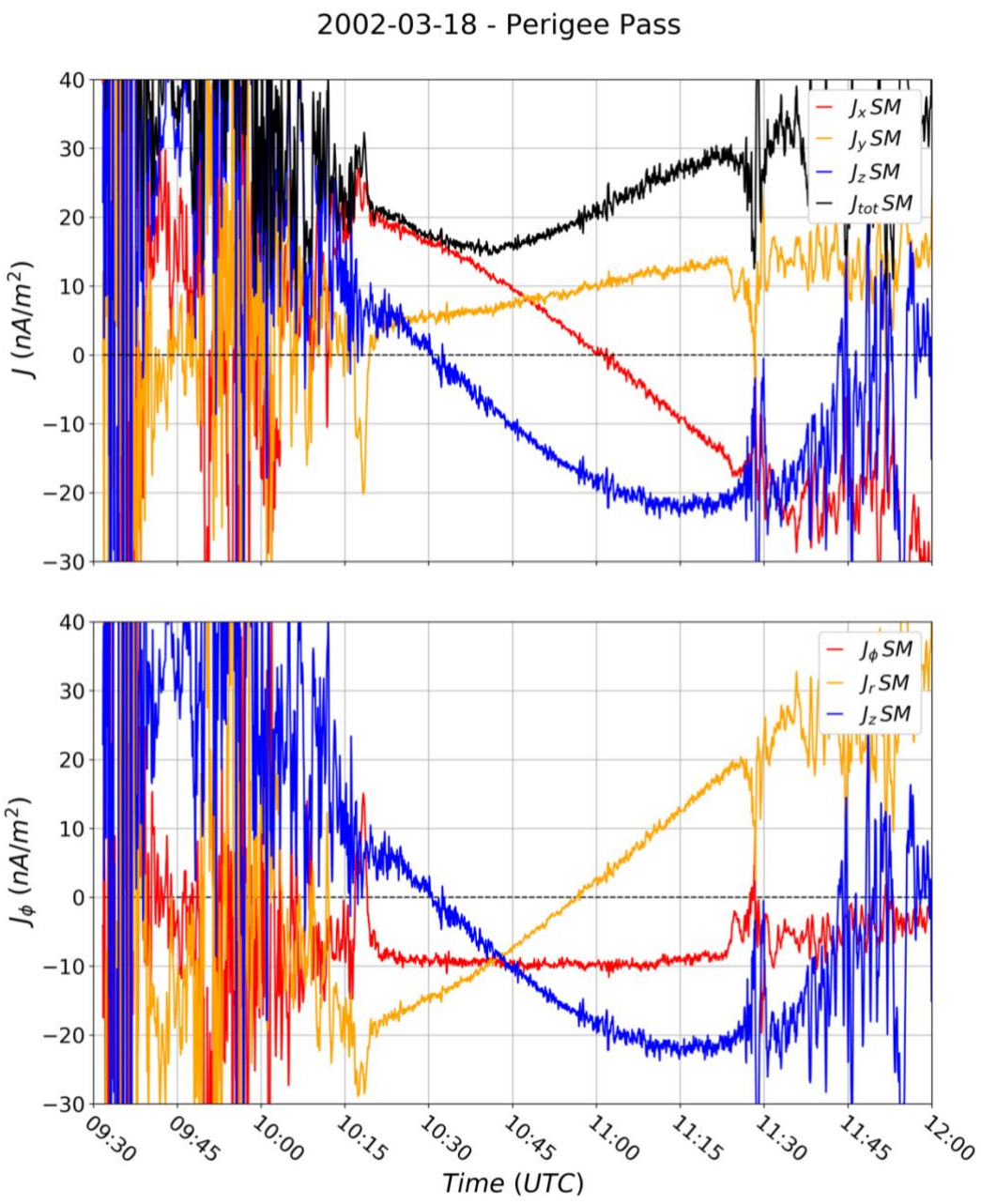

Figure S16. Curlometer currents output from the 18 March 2002 perigee pass. This figure is constructed in the same manner as Figure 9 in Vallat et al. (2005). Note that this figure has the signs of some components reversed to match the convention used in that paper.

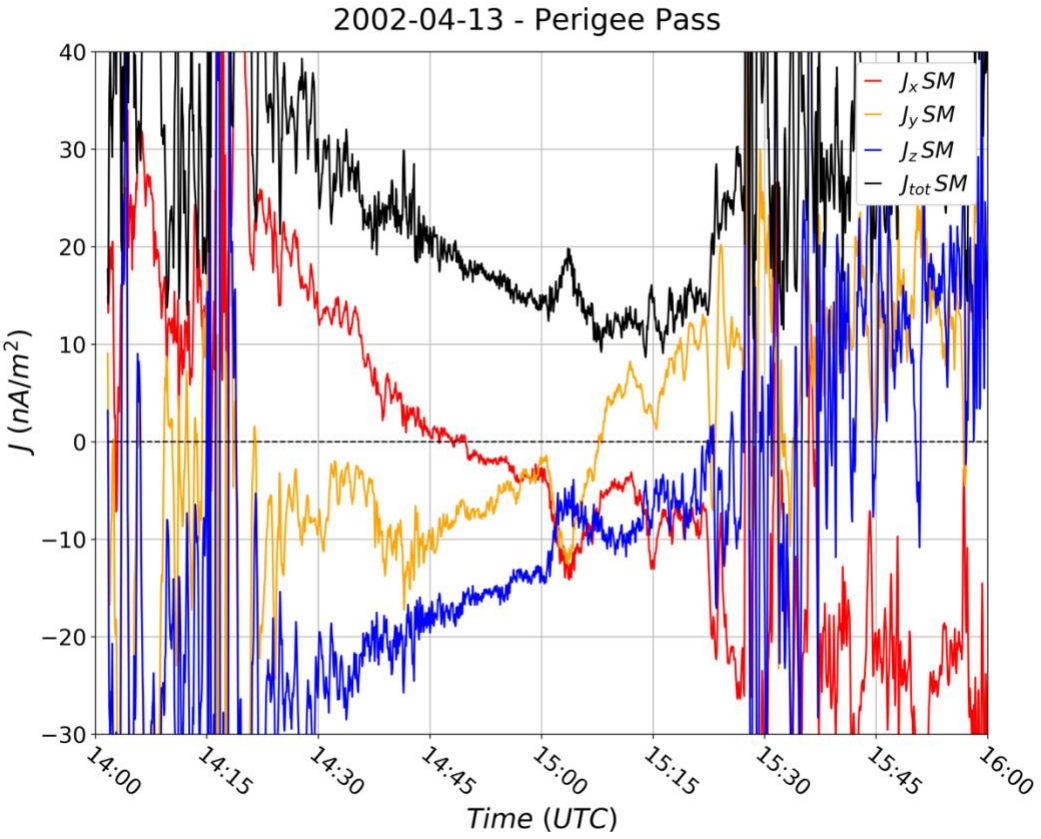

Figure S17. Curlometer currents output from the 13 April 2002 perigee pass. This figure is constructed in the same manner as Figure 2 in Vallat et al. (2005). Note that this figure has the signs of some components reversed to match the convention used in that paper.

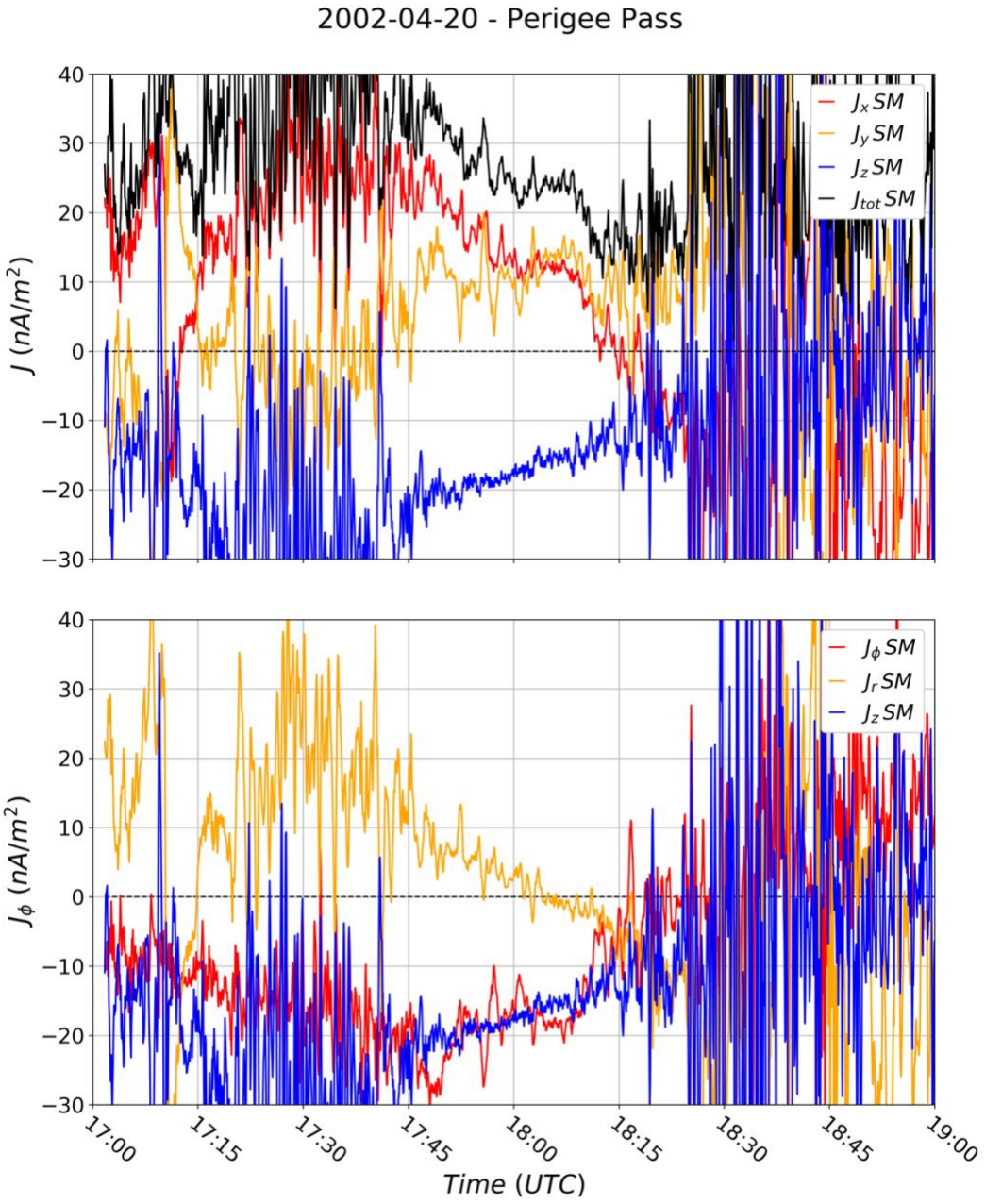

Figure S18. Curlometer currents output from the 20 April 2002 perigee pass. This figure is constructed in the same manner as Figure 14 in Vallat et al. (2005). Note that this figure has the signs of some components reversed to match the convention used in that paper.

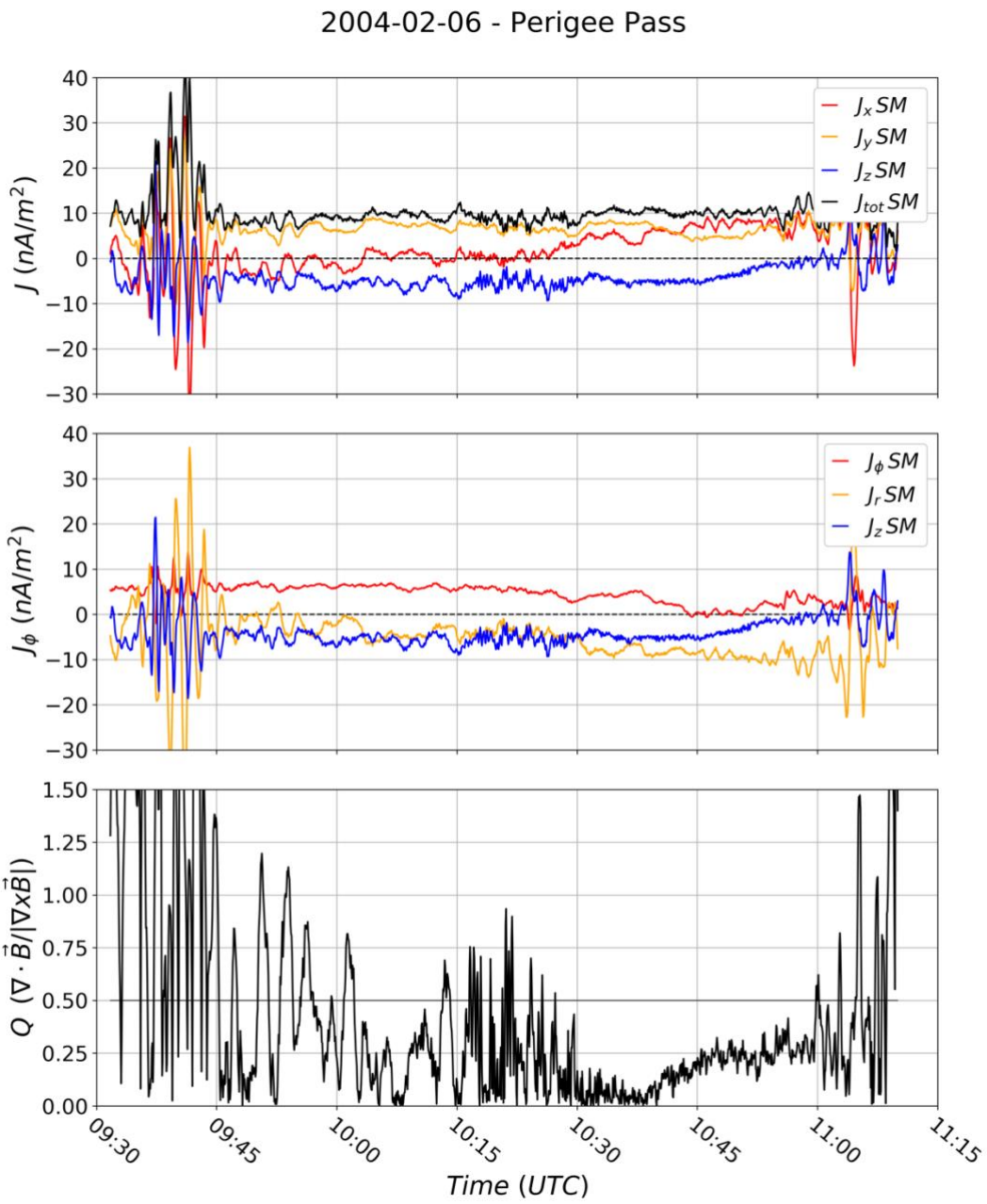

Figure S19. Curlometer currents output from the 6 February 2004 perigee pass. This figure is constructed in the same manner as Figure 2 in Zhang et al. (2011).

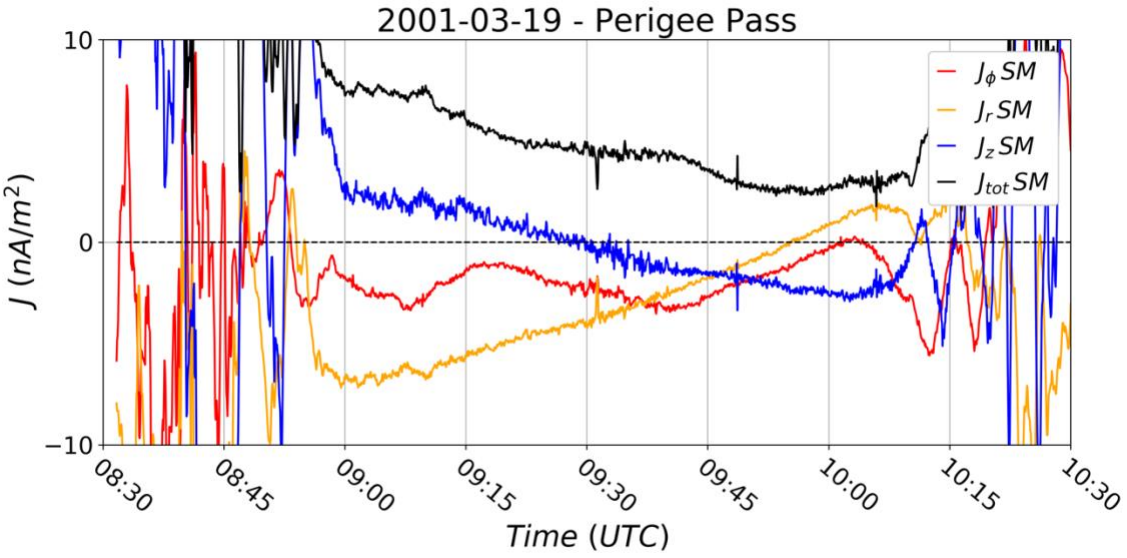

Figure S20. Curlometer currents output from the 19 March 2001 perigee pass. This figure is constructed in the same manner as Figure 9 in Shen et al. (2014).

Movie S1. Tetrahedron rotation for the 10 October 2003 perigee pass. This animation shows rotation of all spacecraft together around the tetrahedron barycenter, and the effect on curlometer output of a simulated current environment. Note that, depending on orientation with respect to a stationary current structure and magnetic topology, the exact same tetrahedron shape and size can produce very different current outputs. Two still frames from this animation are provided in the paper as Figure 4, to highlight the extrema of the animation.

Movie S2. Tetrahedron rotation for the 18 March 2002 perigee pass. This animation shows rotation of all spacecraft together around the tetrahedron barycenter, and the effect on curlometer output of a simulated current environment. Contrary to Movie S1, this event is from 2002, which has a much smaller tetrahedron size. Thus, in the exact same simulated current sheet, the smaller tetrahedron does not produce a large false current at any rotation. However, events from this timeframe make up a small subset of the existing curlometer analysis in the literature.